

Letter

pubs.acs.org/ac

Multishell Au/Ag/SiO₂ Nanorods with Tunable Optical Properties as Single Particle Orientation and Rotational Tracking Probes

- 3 Kuangcai Chen, † Chia-Cheng Lin, † Javier Vela, * and Ning Fang *
- 4 Ames Laboratory, U.S. Department of Energy, and Department of Chemistry, Iowa State University, Ames, Iowa 50011, United States
- 5 Supporting Information

6

8

9

10

11

12

13

14

15

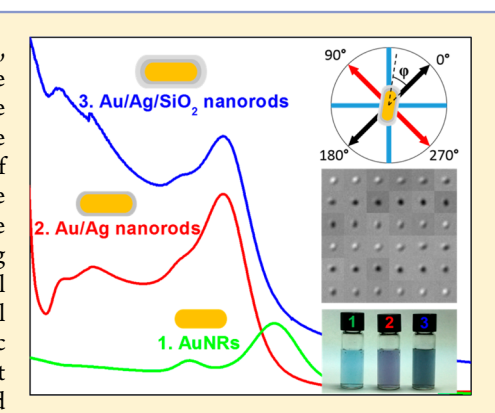
16

17

18

19

ABSTRACT: Three-layer core—shell plasmonic nanorods (Au/Ag/SiO₂—NRs), consisting of a gold nanorod core, a thin silver shell, and a thin silica layer, were synthesized and used as optical imaging probes under a differential interference contrast microscope for single particle orientation and rotational tracking. The localized surface plasmon resonance modes were enhanced upon the addition of the silver shell, and the anisotropic optical properties of gold nanorods were maintained. The silica coating enables surface functionalization with silane coupling agents and provides enhanced stability and biocompatibility. Taking advantage of the longitudinal LSPR enhancement, the orientation and rotational information on the hybrid nanorods on synthetic lipid bilayers and on live cell membranes were obtained with millisecond temporal resolution using a scientific complementary metal-oxide-semiconductor camera. The results demonstrate that the as-synthesized hybrid nanorods are promising imaging probes with improved sensitivity and good biocompatibility for single plasmonic particle tracking experiments in biological systems.



21 Single particle tracking (SPT) is a powerful tool to study the
22 dynamics of cellular and molecular processes, such as
23 membrane dynamics, 1,2 viral infection, and intracellular
24 transport. 4,5 A large collection of imaging probes, including
25 fluorescent molecules, 1,0 quantum dots, 1,0 and plasmonic
26 nanoparticles, 1,10 has been visualized with the aid of various
27 optical microscopy techniques. While it has become a routine
28 practice in SPT experiments to identify the trajectory of an
29 imaging probe, it is more difficult to resolve the dipole
30 orientation of the probe in real time, which may be essential in
31 understanding the underlying biological functions. Recently,
32 considerable efforts have been made to overcome this
33 challenge. Techniques such as fluorescence polarization
34 microscopy, 1,0 dark field polarization scattering, 1,0 defocused
35 orientation and position imaging, 2,1 photothermal imaging, 2,1 orientation spectroscopy, 1,1 total internal reflection scattering
36 correlation spectroscopy, 1,1 total internal reflection scattering
37 microscopy, 1,1 and differential interference contrast (DIC)
38 microscopy, 1,1 have been developed for single particle
39 orientation and rotational tracking, which was coined as
40 SPORT.

Gold nanorods (AuNRs) have been used extensively in SPORT experiments because of their high photostability, good biocompatibility, and most importantly, anisotropic optical properties arising from their localized surface plasmon resonance (LSPR). Great success has been achieved on the AuNR synthesis using seed-mediated methods to fabricate a variety of AuNRs with different sizes and aspect ratios and thus the resulting tunable extinction spectra across a wide spectral range. Compared with gold nanocrystals of similar size, silver nanocrystals exhibit stronger LSPR responses with more intense electric field enhancement and stronger absorption and

scattering. However, the synthesis of anisotropic silver 52 nanorods (AgNRs), especially for the smaller sizes (<100 nm 53 in length) that are better suited for biological studies, is more 54 difficult than that of AuNRs in terms of size and shape 55 uniformity control. Since silver shares the same face 56 centered cubic crystal structure with gold and their lattice 57 mismatch is as small as 0.27%, AuNRs are suitable templates for 58 epitaxial silver growth to form Au/Ag core—shell nanorods 59 (Au/AgNRs). The optical properties of Au/AgNRs can be 60 finely tuned by controlling the aspect ratio of the AuNR cores 61 and the amount of silver grown on the gold surface. Moreover, the formation of Au/AgNRs induces multiple 63 plasmonic bands that differ from single-component nanocrystals.

In view of the intrinsic cytotoxicity and instable nature of the 66 silver shells in aqueous solution, 23,31,32 encapsulation of Au/ 67 AgNRs within a thin silica layer to form a three-layer core—shell 68 nanorod structure, which will be referred to as Au/Ag/SiO $_2$ — 69 NR in this Letter, can provide the necessary protection in 70 biological imaging applications. The silica coating also improves 71 the colloidal stability of Au/AgNRs, maintains the rod shape, 72 and enables further surface functionalization with silane 73 coupling agents for potential bioconjugation. $^{33-35}$ Surface 74 modification of the silica shell usually involves covalent 75 attachment; therefore, this avoids cysteine residue replacement 76

Received: February 12, 2015 Accepted: April 7, 2015



Analytical Chemistry Letter

77 of thiol ligands, which is often used in gold or silver surface 78 functionalization. ³⁶

In the present study, Au/Ag/SiO₂—NRs were synthesized and tested for SPORT experiments. Millisecond/submillist second temporal resolution was achieved in imaging the fast dynamics of Au/Ag/SiO₂—NRs rotating on synthetic lipid membranes and live cell membranes. To the best of our knowledge, this study demonstrates for the first time the development and application of hybrid core—shell nanorods as a new type of rotational probe.

The first step in synthesizing $Au/Ag/SiO_2$ –NRs was to 88 prepare AuNRs using a seed-mediated growth method in 89 aqueous solution utilizing cetyltrimethylammonium bromide 90 (CTAB) as capping agent to maintain colloidal stability. The 91 average diameter, length, and aspect ratio of the synthesized 92 AuNRs obtained from the TEM images (Figure S1 in the 93 Supporting Information) were 22.8 \pm 3.2 nm, 52.6 \pm 7.2 nm, 94 and 2.3 \pm 0.2, respectively. Their transverse and longitudinal 95 LSPR wavelengths were centered at 517 and 632 nm, as shown 96 in the UV–vis extinction spectrum (Figure 1, green curve).

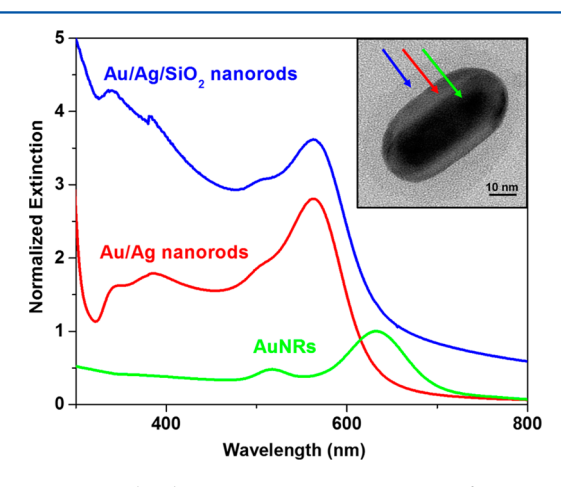


Figure 1. Normalized UV–vis extinction spectra of AuNRs, Au/AgNRs, and Au/Ag/SiO₂–NRs in water. All the spectra are normalized to the longitudinal dipolar plasmonic peak at 632 nm. The inset is a representative TEM image of Au/Ag/SiO₂–NR and the colored arrows indicate gold-only (green), silver-coated (red), and silica-coated (blue) samples.

In the second step of synthesis, a thin silver layer (~7 nm 98 thick) was deposited onto the AuNRs following a published 99 procedure. 25,37 The thickness of the silver coating was 100 controlled by adjusting the amount of AgNO₃ precursor. 101 Upon the addition of silver onto the AuNR cores, the 102 extinction peak at the lowest energy wavelength was blue-103 shifted and new plasmonic bands appeared at higher energies. 104 Figure S2 in the Supporting Information illustrates the UV-vis extinction spectra of the Au/AgNRs with three Ag/Au molar 106 ratios of 0.11, 0.22, and 0.34. As the Ag/Au molar ratio 107 increases, the silver shell becomes thicker and the longitudinal LSPR wavelength is blue-shifted from 632 nm to 575, 537, and 109 503 nm, respectively. This blue shift is attributed to the reduced 110 aspect ratio of the nanorods after the silver coating and the 111 increased silver loading on gold dominates the optical 112 properties. This plasmonic band shift can be used to estimate the Ag shell thickness as well as to direct further the syntheses. 26,28,30 The Au/AgNRs with the Ag/Au molar ratio 115 of 0.11 maintained the original cylindrical rod shape. Figure S2 116 curve b in the Supporting Information shows the four

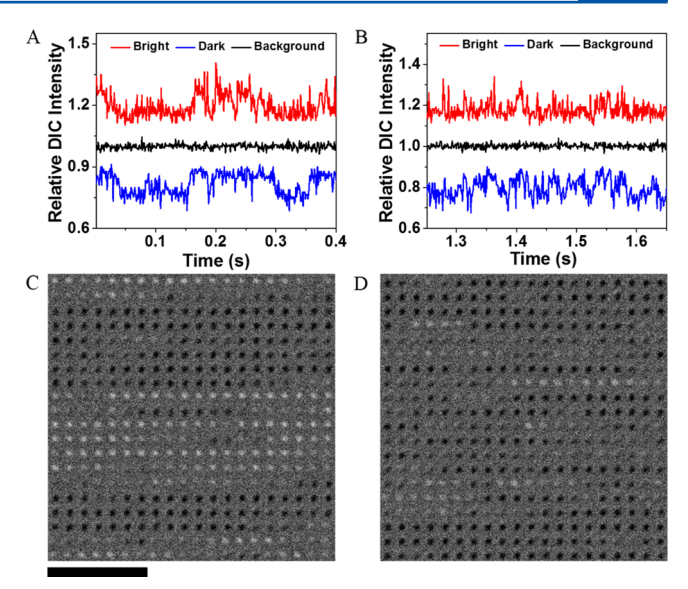


Figure 2. Relative DIC intensity traces of (A) slow rotation and (B) fast rotation, corresponding to the shaded gray and green areas in Figure S5 in the Supporting Information. Four hundred (400) consecutive recorded DIC images for (A) and (B) are stitched together (from left to right and from top to bottom) and shown as (C) and (D), respectively. Scale bar is 5 μ m.

plasmonic bands at 339, 400, 506, and 563 nm. The rise of 117 two higher energy bands at shorter wavelengths is believed to 118 be due to the octupolar plasmonic modes, with the peaks at 506 119 and 575 nm corresponding to the transverse and longitudinal 120 dipolar plasmonic modes. ^{25,27,28} At higher Ag/Au molar ratios, 121 the rod shape was no longer maintained and a large fraction of 122 irregular silver shells was observed (data not shown). Only the 123 rod-shaped Au/AgNRs made with the Ag/Au molar ratio of 124 0.11 were used in the following synthesis and imaging 125 experiments.

In order to improve the stability and reduce the intrinsic 127 toxicity of silver, a dense silica layer was added as the last 128 synthetic step. Figure 1 compares the normalized UV-vis 129 extinction spectra of AuNRs, Au/AgNRs, and Au/Ag/SiO₂- 130 NRs. In these measurements, the colloidal solutions were kept 131 at the same concentration to minimize the dilution effect. 132 Figure 1 (inset) shows a representative TEM image of the 133 core-shell structure with average dimensions of ~46 nm × 64 134 nm. Due to the relatively low lattice mismatch (0.27%) of the 135 two metals, the Ag shells grow almost perfectly upon the 136 AuNRs through epitaxial deposition. We also found that the Ag 137 shell thickness increases faster along the lateral direction than at 138 the tips, which leads to the reduction of the aspect ratio of Au/ 139 AgNRs from the original AuNRs. In view of their relative 140 extinction intensities, the longitudinal dipolar plasmonic mode 141 increases by roughly a factor of 3 in Au/AgNRs compared to 142 that of the original AuNRs. The baseline in the UV-vis 143 extinction spectrum of the Au/Ag/SiO2-NR solution is 144 elevated because of scattering caused by silica, as reported 145 previously.3

Following the synthesis, the $Au/Ag/SiO_2$ -NRs were imaged 147 under a DIC microscope equipped with a Hamamatsu ORCA- 148 Flash 2.8 scientific CMOS camera, which allows imaging at 149 millisecond or submillisecond temporal resolution. In addition 150 to the enhanced LSPR response from the silver coating, the 151 blue shift of the LSPR wavelength from 632 nm (AuNRs) to 152

Analytical Chemistry Letter

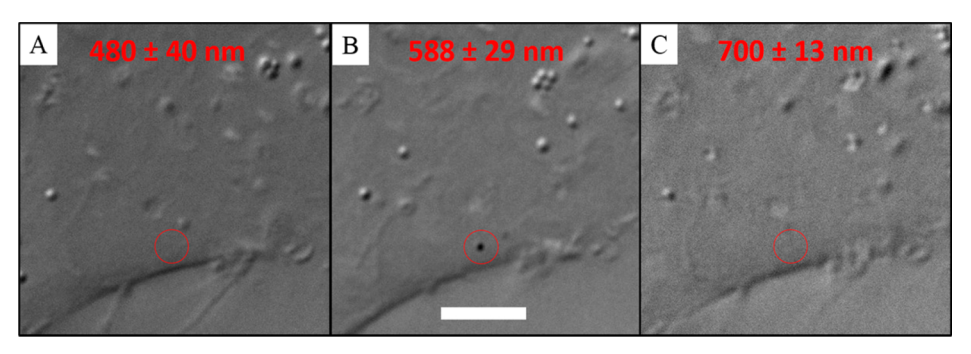


Figure 3. Differentiation of the $Au/Ag/SiO_2$ -NRs (highlighted in the red circles) from other cellular features using three filters, (A) 480 ± 40 nm, (B) 588 ± 29 nm, and (C) 700 ± 13 nm. Scale bar is 4 μ m. These images were taken sequentially. The nanorod and many cellular features changed their location and/or morphology during the imaging time.

153 563 nm provides another noticeable gain in the camera's 154 quantum efficiency and therefore sensitivity.

In our previous studies, the DIC contrasts, defined as the difference between the brightest and the darkest intensities divided by the average local background intensity, of nano-158 particles were shown to be wavelength dependent and the longitudinal LSPR was more sensitive to the environment than the transverse LSPR. ^{18,38} Herein, the DIC contrast of an immobilized, randomly oriented Au/Ag/SiO₂–NR is plotted as for a function of excitation wavelength (Figure S3 in the Supporting Information). The highest DIC contrast for this particle was found when a 585 \pm 29 nm filter was used for life illumination, which corresponds to the longitudinal dipolar plasmonic band.

DIC images of two immobilized Au/Ag/SiO₂-NRs on glass 167 168 slides were recorded at different exposure times and stitched together to make Movie S1 in the Supporting Information, 170 which is played at 30 frames per second (fps). These two 171 particles in the movie were nearly perpendicular to each other 172 as their DIC images showed the totally bright and totally dark patterns. During these measurements, the light source was kept at the maximum output power (100 W), and the overall intensity decreased linearly as expected when shorter exposure 176 time was used (Figure S4 in the Supporting Information). The relative bright and dark intensity measurement errors were increased from ~1% at 50 ms to ~5% at 0.5 ms for both nanorods (Table S1 in the Supporting Information). Because of 180 the LSPR enhancement due to the silver coating, the coreshell hybrid nanorods were detectable at a temporal resolution 182 as fast as 0.5 ms, which is approximately an order of magnitude faster than the previously reported fastest temporal resolution of 2-5 ms.^{5,19}

A 360° rotation study of the Au/Ag/SiO₂—NRs was carried out by rotating the sample stage with 10° increments to position the nanorods in different orientations while exciting at the longitudinal LSPR wavelength of 563 nm. The orientation angle φ was defined as the angle between the long axis of the nanorod and the "bright" polarization direction of the DIC microscope (Figure S5A in the Supporting Information). The "bright" polarization direction is named after the fact that a completely bright DIC image is obtained when the nanorod's long axis aligns with this polarization direction (φ = 0), while the "dark" polarization direction corresponds to a completely dark DIC image. Figure S5B in the Supporting Information shows the complete rotation set of disproportionate bright and dark DIC image patterns. The DIC images change periodically set the nanorod's long axis rotates against the polarization

directions. This is in good agreement with the polarization- $_{200}$ dependent rotation behaviors of plasmonic nanoparticles that $_{201}$ have been extensively investigated in gold nanorods and $_{202}$ nanowires. $_{18,39}^{18,39}$ In view of the periodic changes, a correlation $_{203}$ between the bright and dark intensity traces is observed: the $_{204}$ bright and dark intensities increase and decrease in the same $_{205}$ direction. This orientation/polarization dependence is the $_{206}$ foundation for the use of Au/Ag/SiO $_{2}$ –NRs as SPORT probes. $_{207}$

Dynamic tracking of the $Au/Ag/SiO_2$ –NRs was first $_{208}$ performed on synthetic lipid bilayers. The nanorods were $_{209}$ introduced onto the synthetic lipid bilayers in a chamber and $_{210}$ bound to the membrane through nonspecific interactions. $_{211}$ Movies were recorded at a temporal resolution of 1 ms under $_{212}$ $_{588}$ \pm 29 nm illumination. Figure S6 in the Supporting $_{213}$ Information shows the DIC intensity traces extracted from a $_{214}$ representative 4 s (4000 frames) movie. The autocorrelation $_{215}$ analysis of the DIC bright and dark traces $_{19}$ reveals that the $_{216}$ nanorod's rotation speed fluctuates constantly. Representative $_{217}$ examples of slow and fast rotation are given in Figure 2. The $_{218}$ figure $_{219}$ mean relaxation times of these two cases are $_{19}$ s (slow) and $_{219}$ 0.024 s (fast).

To demonstrate the suitability of the new rotational probes 221 for live-cell imaging, A549 human lung cancer cells were used 222 as a model system, which provided a dynamic surface for 223 rotational studies. Despite the much more complex cellular 224 environments, the wavelength dependent properties of these 225 SPORT probes are easily distinguishable from other cellular 226 features by using different band-pass filters. Three band-pass 227 filters (480 \pm 40 nm, 588 \pm 29 nm, and 700 \pm 13 nm) were 228 used to identify the nanorods. As shown in Figure 3, the 588 \pm 229 f3 and in a high-contrast DIC image of Au/Ag/SiO2-NRs that is 231 distinct from the background. With either 480 \pm 40 nm or 700 232 \pm 13 nm band-pass filters, the Au/Ag/SiO2-NRs disappear 233 into the background due to the low contrast achieved at these 234 wavelengths, which are far away from the LSPR bands.

In the live-cell imaging experiments, the Au/Ag/SiO₂–NRs 236 were added into a chamber with A549 cells attached on the 237 coverslip. Movies of the dynamic rotation of these nanorods 238 were recorded at different exposure times of 1, 5, and 50 ms. 239 The DIC intensity traces and the corresponding sets of 240 consecutive DIC images were plotted in Figure S7 in the 241 Supporting Information. The autocorrelation analysis of the 242 DIC bright and dark traces gives mean relaxation times of 11 243 ms at the temporal resolution of 1 ms, 23 at 5 ms, and 115 at 50 244 ms. Higher temporal resolution helps to unveil fast rotational 245

Analytical Chemistry Letter

246 dynamics, even though the overall intensity inevitably decreases 247 as the single-frame exposure time decreases.

In summary, we have successfully synthesized Au/Ag/SiO₂—249 NRs with well-controlled size and shape for SPORT. These optically anisotropic hybrid plasmonic nanorods exhibit in DIC microscopy. With the enhancement of the longitudinal dipolar LSPR after silver coating, these nanorods provide sufficient sensitivity for detection at millisecond temporal resolution on both synthetic lipid bilayers and live cell membranes. Surface modification of the silica layer of the hybrid nanorods will enable versatile applications in SPORT.

ASSOCIATED CONTENT

259 Supporting Information

260 Experimental details, additional figures, and a movie as 261 mentioned in the text. This material is available free of charge 262 via the Internet at http://pubs.acs.org.

63 AUTHOR INFORMATION

264 Corresponding Authors

- 265 *E-mail: vela@iastate.edu.
- 266 *E-mail: nfang@iastate.edu.

267 Author Contributions

⁷K.C. and C.-C.L. contributed equally to this work.

260 Notes

270 The authors declare no competing financial interest.

71 ACKNOWLEDGMENTS

272 This research is supported by the U.S. Department of Energy, 273 Office of Basic Energy Sciences, Division of Chemical Sciences, 274 Geosciences, and Biosciences through the Ames Laboratory. 275 The Ames Laboratory is operated for the U.S. Department of 276 Energy by Iowa State University under Contract No. DE-277 AC02-07CH11358. The authors thank Michelle Thompson for 278 assistance.

279 REFERENCES

- 280 (1) Saxton, M. J.; Jacobson, K. Annu. Rev. Biophys. Biomol. Struct. 281 1997, 26, 373–399.
- 282 (2) Fujiwara, T.; Ritchie, K.; Murakoshi, H.; Jacobson, K.; Kusumi, A. 283 *J. Cell Biol.* **2002**, *157*, 1071–1081.
- 284 (3) Lakadamyali, M.; Rust, M. J.; Babcock, H. P.; Zhuang, X. Proc. 285 Natl. Acad. Sci. U.S.A. 2003, 100, 9280–9285.
- 286 (4) Yezhelyev, M. V.; Qi, L.; O'Regan, R. M.; Nie, S.; Gao, X. J. Am. 287 Chem. Soc. 2008, 130, 9006–9012.
- 288 (5) Gu, Y.; Sun, W.; Wang, G.; Jeftinija, K.; Jeftinija, S.; Fang, N. *Nat.* 289 *Commun.* **2012**, *3*, 1030.
- 290 (6) Greeson, J. N.; Raphael, R. M. J. Biomed. Opt. **200**7, 12, 021002–291 021009.
- (7) Beausang, J. F.; Sun, Y.; Quinlan, M. E.; Forkey, J. N.; Goldman,
- 293 Y. E. Cold Spring Harbor Protoc. 2012, 2012, 535-545.
 294 (8) Chung, I.; Shimizu, K. T.; Bawendi, M. G. Proc. Natl. Acad. Sci.
 295 U.S.A. 2003, 100, 405-408.
- 296 (9) Toprak, E.; Enderlein, J.; Syed, S.; McKinney, S. A.; Petschek, R. 297 G.; Ha, T.; Goldman, Y. E.; Selvin, P. R. *Proc. Natl. Acad. Sci. U.S.A.* 298 **2006**, *103*, 6495–6499.
- 299 (10) Sönnichsen, C.; Alivisatos, A. P. Nano Lett. 2004, 5, 301-304.
- 300 (11) Chang, W.-S.; Ha, J. W.; Slaughter, L. S.; Link, S. *Proc. Natl.* 301 Acad. Sci. U.S.A. **2010**, 107, 2781–2786.
- 302 (12) Tcherniak, A.; Dominguez-Medina, S.; Chang, W.-S.; Swanglap, 303 P.; Slaughter, L. S.; Landes, C. F.; Link, S. *J. Phys. Chem. C* **2011**, *115*, 304 15938–15949.

(13) Li, T.; Li, Q.; Xu, Y.; Chen, X. J.; Dai, Q. F.; Liu, H.; Lan, S.; 305 Tie, S.; Wu, L. J. ACS Nano 2012, 6, 1268-1277. (14) Zhang, B.; Lan, T.; Huang, X.; Dong, C.; Ren, J. Anal. Chem. 307 2013, 85, 9433-9438. (15) Marchuk, K.; Ha, J. W.; Fang, N. Nano Lett. 2013, 13, 1245- 309 1250. (16) Stender, A. S.; Marchuk, K.; Liu, C.; Sander, S.; Meyer, M. W.; 311 Smith, E. A.; Neupane, B.; Wang, G.; Li, J.; Cheng, J.-X.; Huang, B.; 312 Fang, N. Chem. Rev. 2013, 113, 2469-2527. (17) Ha, J. W.; Marchuk, K.; Fang, N. Nano Lett. 2012, 12, 4282-314 315 (18) Wang, G.; Sun, W.; Luo, Y.; Fang, N. J. Am. Chem. Soc. 2010, 316 132, 16417-16422. (19) Gu, Y.; Sun, W.; Wang, G.; Fang, N. J. Am. Chem. Soc. 2011, 318 133, 5720-5723. 319 (20) Gu, Y.; Ha, J. W.; Augspurger, A. E.; Chen, K.; Zhu, S.; Fang, N. 320 Nanoscale 2013, 5, 10753-10764. 321 (21) Nikoobakht, B.; El-Sayed, M. A. Chem. Mater. 2003, 15, 1957- 322 1962. 323 (22) Gole, A.; Murphy, C. J. Chem. Mater. 2004, 16, 3633-3640. (23) Jana, N. R.; Gearheart, L.; Murphy, C. J. Chem. Commun. 2001, 325 326 617 - 618(24) Pietrobon, B.; McEachran, M.; Kitaev, V. ACS Nano 2008, 3, 327 328 (25) Liu, M.; Guyot-Sionnest, P. J. Phys. Chem. B 2004, 108, 5882- 329 5888 330 (26) Xiang, Y.; Wu, X.; Liu, D.; Li, Z.; Chu, W.; Feng, L.; Zhang, K.; 331 Zhou, W.; Xie, S. Langmuir 2008, 24, 3465-3470. (27) Park, K.; Drummy, L. F.; Vaia, R. A. J. Mater. Chem. 2011, 21, 333 15608-15618. 334 (28) Jiang, R.; Chen, H.; Shao, L.; Li, Q.; Wang, J. Adv. Mater. 2012, 335 24, OP200-OP207. (29) Hou, S.; Hu, X.; Wen, T.; Liu, W.; Wu, X. Adv. Mater. 2013, 25, 337 3857-3862. 338 (30) Zhu, J.; Zhang, F.; Li, J.-J.; Zhao, J.-W. Gold Bull. 2014, 47, 47–339 55. (31) Damm, C.; Segets, D.; Yang, G.; Vieweg, B. F.; Spiecker, E.; 341 Peukert, W. Small 2011, 7, 147-156. 342 (32) Cheng, X.; Zhang, W.; Ji, Y.; Meng, J.; Guo, H.; Liu, J.; Wu, X.; 343 Xu, H. RSC Adv. 2013, 3, 2296-2305. 344 (33) Kobayashi, Y.; Katakami, H.; Mine, E.; Nagao, D.; Konno, M.; 345 Liz-Marzán, L. M. J. Colloid Interface Sci. 2005, 283, 392-396. 346 (34) Sendroiu, I. E.; Warner, M. E.; Corn, R. M. Langmuir 2009, 25, 347 11282-11284. 348 (35) Mahanti, M.; Basak, D. RSC Adv. 2014, 4, 15466-15473. 349 (36) Aryal, S.; R, B. K. C.; Dharmaraj, N.; Bhattarai, N.; Kim, C. H.; 350 Kim, H. Y. Spectrochim. Acta, Part A 2006, 63, 160-163. 351 (37) Khalavka, Y.; Becker, J.; Sonnichsen, C. J. Am. Chem. Soc. 2009, 352 131, 1871-1875. 353

(38) Ha, J. W.; Sun, W.; Stender, A. S.; Fang, N. J. Phys. Chem. C 354

(39) Ha, J. W.; Chen, K.; Fang, N. Chem. Commun. 2013, 49, 11038-356

2012, 116, 2766-2771.

11040.

355

357